

# Modifications of the Rho Meson from the Virtual Pion Cloud in Hot and Dense Matter

M. Urban<sup>1</sup>, M. Buballa<sup>1</sup>, R. Rapp<sup>2</sup> and J. Wambach<sup>1</sup>

1) *Inst. f. Kernphysik, TU Darmstadt, Schloßgartenstr. 9, 64289 Darmstadt, Germany*

2) *Department of Physics and Astronomy, State University of New York, Stony Brook, NY 11794-3800, U.S.A.*

## Abstract

The modification of the  $\rho$ -meson self-energy due to the coupling to in-medium pions is calculated consistently at finite baryon density and temperature, keeping the full 3-momentum dependence in a gauge invariant way. As a function of nucleon density, the  $\rho$ -meson spectral function is strongly enhanced in the invariant mass region  $M \lesssim 650$  MeV, while the maximum, i.e. the pole mass, is slightly shifted upwards. As a function of temperature, for fixed nucleon density, the imaginary part of the self-energy increases further due to Bose-enhancement. At the same time the mass shift from the real part becomes very large. As a consequence of these medium effects, the dilepton rate in the low-mass region  $M \lesssim 650$  MeV increases strongly, while the peak at  $M \approx 770$  MeV disappears.

# 1 Introduction

In the last few years the spectra of dilepton pairs ( $e^+e^-$  or  $\mu^+\mu^-$ ) emerging from (ultra-) relativistic heavy-ion collisions have been measured in various experiments. Despite of low production rates, resulting in large statistical errors, dileptons have the distinct advantage of reaching the detector almost undisturbed and are therefore, in principle, ideal probes for studying the hot and dense initial phases of the fireball [1].

The dilepton production rate in a hot and dense medium is directly related to the electromagnetic current-current correlation function. In the hadronic phase of the fireball and in the low invariant-mass region,  $M \lesssim 1$  GeV ( $M =$  invariant mass of the dilepton pair), this correlation function is largely saturated by the  $\rho$ -,  $\omega$ - and  $\phi$ -mesons through vector-meson dominance [2, 3]. Hence dilepton spectra contain information about the properties (mass, width) of these mesons in the surrounding medium, most prominently the  $\rho$  meson due to its relatively large dilepton decay width (see [4] for a recent review).

From a field theoretical point of view, the modifications of the  $\rho$ -meson properties are described by its self-energy, which contains all interactions with the surrounding matter. In vacuum the  $\rho$ -meson receives a width of  $\approx 150$  MeV from the decay into two pions, corresponding to the self-energy diagram  $\Sigma_{\rho\pi\pi}$ , shown in Fig. 1a. In cold nuclear matter pions are strongly modified by Delta-hole ( $\Delta h$ ) excitations as evidenced from the wealth of pion-nucleus data [5]. It is therefore suggestive to include medium modifications by replacing the free pions in  $\Sigma_{\rho\pi\pi}$ , by in-medium ones [6, 7, 8, 9]. Of course the  $\rho$ -meson can also interact resonantly with the nucleons as described by the self-energy contributions shown in Fig. 1b and denoted by  $\Sigma_{\rho B}$  [10, 11]. At finite temperature self-energy contributions  $\Sigma_{\rho M}$ , such as the one shown in Fig. 1c describing direct interactions with thermal mesons, need to be considered in addition. Combining these three self-energy contributions,  $\Sigma_{tot} = \Sigma_{\rho\pi\pi} + \Sigma_{\rho B} + \Sigma_{\rho M}$ , a reasonable description of the dilepton spectra measured by the CERES collaboration [12] emerges [13, 14]. In this description the  $\rho$ -meson acquires a substantial width and ceases to be a well-defined quasiparticle [4].

In the present article we will concentrate on the contribution  $\Sigma_{\rho\pi\pi}$ , which is probably the most difficult part. In the first calculations of  $\Sigma_{\rho\pi\pi}$  in matter, the flat dispersion relation of the in-medium pions produced a divergence of  $\Sigma_{\rho\pi\pi}$  near the two pion threshold [6]. However, gauge invariance was violated in these calculations. To correct this, appropriate  $\rho\pi\pi$  vertex corrections had to be included, which cancel the divergence [7, 8, 9]. Chanfray

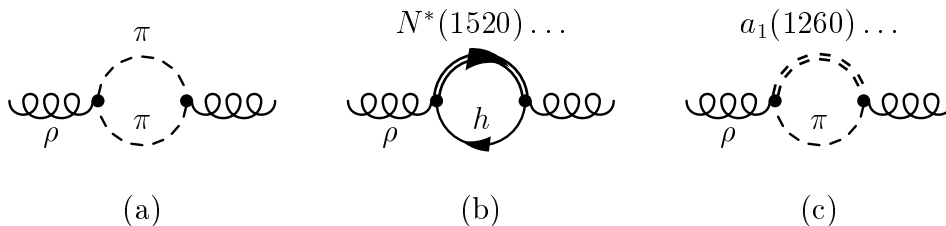


Figure 1: Examples for different contributions to the  $\rho$ -meson self-energy  $\Sigma_{tot}$  in hadronic matter: (a) Decay into two pions,  $\Sigma_{\rho\pi\pi}$ . (b) Excitation of baryonic resonances via  $\rho N$  scattering in baryon rich matter,  $\Sigma_{\rho B}$ . (c) Excitation of mesonic resonances in  $\rho\pi$  scattering in a hot meson gas,  $\Sigma_{\rho M}$ .

and Schuck [8] and Herrmann et al. [9] restricted themselves to  $\rho$ -mesons at rest and zero temperature. In Ref. [15] we presented an extension of their models to  $\rho$ -mesons in cold nuclear matter with finite 3-momentum. When applied to photoabsorption cross sections for nucleons and nuclei [16], it was found that the pion-nucleon and pion-Delta form factors had to be chosen rather soft, resulting in reduced in-medium contributions from  $\Sigma_{\rho\pi\pi}$ .

For a consistent calculation of dilepton rates it is important to include also temperature. This is the aim of the present article. We start with a brief description of our model for  $\Sigma_{\rho\pi\pi}$  without baryons, i.e. in vacuum or in a hot meson gas. Section 3 discusses the medium modifications of the pion propagator in hot baryon rich matter, which will be used in Section 4 to calculate  $\Sigma_{\rho\pi\pi}$  at finite temperature and baryon density. The combined effects of temperature and baryon density on dilepton and photon rates are studied in Section 5.

## 2 The $\rho$ -meson in a hot pion gas

Before taking into account baryonic effects, we briefly discuss the  $\rho$ -meson self-energy at zero baryon density,  $\varrho_B = 0$ , i.e. in vacuum (temperature  $T = 0$ ) and in a hot pion gas (temperature  $T > 0$ ). Minimal substitution leads to the following  $\pi\rho$ -interaction Lagrangian [9]:

$$\mathcal{L}_{\pi\rho} = \frac{1}{2}ig\rho_\mu(T_3\vec{\phi} \cdot \partial^\mu\vec{\phi} + \partial^\mu\vec{\phi} \cdot T_3\vec{\phi}) - \frac{1}{2}g^2\rho_\mu\rho^\mu T_3\vec{\phi} \cdot T_3\vec{\phi}, \quad (1)$$

where  $\vec{\phi}$  denotes the isovector pion field,  $\rho_\mu$  the field of the neutral  $\rho$ -meson,  $T_3$  the third component of the isospin operator and  $g$  the  $\rho\pi\pi$  coupling constant. The  $\rho$ -meson self-energy  $\Sigma_{\rho\pi\pi}$ , in the following denoted  $\Sigma$  for simplicity, to order  $g^2$  is represented by the two diagrams shown in Figs. 2a and 2b. Calculating these diagrams within the imaginary-time formalism described e.g. in Ref. [17], we finally obtain the following expression for the spatial components ( $i, j = 1, 2, 3$ ) of the retarded  $\rho$ -meson self-energy tensor  $\Sigma_{\mu\nu}$  (see

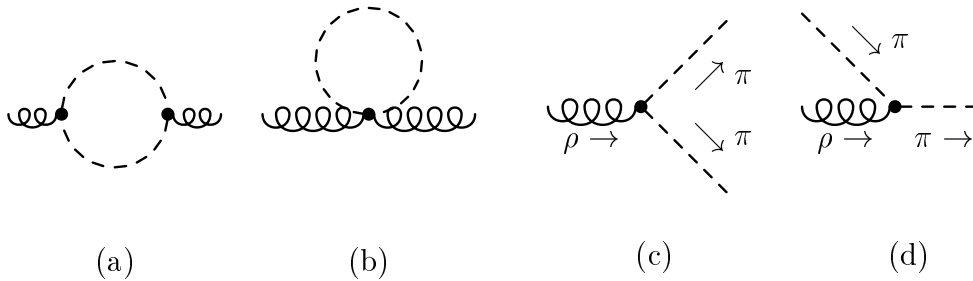


Figure 2: (a) and (b) Diagrams for the  $\rho$ -meson self-energy  $\Sigma_{\rho\pi\pi}$  at zero baryon density. (c) and (d) Processes contributing to the imaginary part of diagram (a) at finite temperature  $T > 0$ : (c)  $\rho \rightarrow \pi + \pi$  (decay of a  $\rho$ -meson into two pions), (d)  $\rho + \pi \rightarrow \pi$  (absorption of a virtual  $\rho$ -meson by a thermal pion).

Section 4 for details):

$$\begin{aligned} \Sigma_{ij}(q_0, \vec{q}) &= g^2 \int \frac{d^3k}{(2\pi)^3} (2k+q)_i (2k+q)_j \left( \frac{(1+2n_{\vec{k}})(\omega_{\vec{k}+\vec{q}} + \omega_{\vec{k}})}{2\omega_{\vec{k}+\vec{q}}\omega_{\vec{k}}((q_0+i\varepsilon)^2 - (\omega_{\vec{k}+\vec{q}} + \omega_{\vec{k}})^2)} \right. \\ &\quad \left. + \frac{n_{\vec{k}}(\omega_{\vec{k}+\vec{q}} - \omega_{\vec{k}})}{\omega_{\vec{k}+\vec{q}}\omega_{\vec{k}}((q_0+i\varepsilon)^2 - (\omega_{\vec{k}+\vec{q}} - \omega_{\vec{k}})^2)} \right) \\ &\quad + g^2 \delta_{ij} \int \frac{d^3k}{(2\pi)^3} \frac{1+2n_{\vec{k}}}{\omega_{\vec{k}}}. \end{aligned} \quad (2)$$

Here we have used the short-hand notation  $\omega_{\vec{k}} = \sqrt{m_\pi^2 + \vec{k}^2}$  and  $n_{\vec{k}} = 1/(e^{\omega_{\vec{k}}/T} - 1)$ .

The self-energy  $\Sigma$  can be separated into vacuum and medium contributions,  $\Sigma = \Sigma^{vac} + \Sigma^{med}$  (terms  $\propto 1$  and  $\propto n_{\vec{k}}$ , respectively). In order to preserve current conservation and Lorentz invariance in the vacuum, the divergent integrals in  $\Sigma^{vac}$  are regularized using the Pauli-Villars scheme. The free parameters of the model (bare  $\rho$  mass  $m_\rho^{(0)} = 853$  MeV, coupling constant  $g = 5.9$  and Pauli-Villars regulator mass  $\Lambda_\rho = 1$  GeV) are adjusted such that the electromagnetic form factor of the pion and the  $\pi\pi$ -scattering phase shifts  $\delta_1^1$  are reproduced satisfactorily (see Ref. [15] for details). Numerical results for  $\Sigma^{vac}$  and the corresponding  $\rho$ -meson spectral function in vacuum are displayed in Fig. 3 (dotted lines).

Let us now discuss the self-energy at finite temperature. As there exists a preferred frame of reference in the heat bath,  $\Sigma$  depends on  $q_0$  and  $\vec{q}$  separately, and splits into 3-dimensionally transverse and longitudinal parts  $\Sigma_T$  and  $\Sigma_L$  [18], which are related to the spatial components of the self-energy tensor by

$$\Sigma_T = \frac{1}{2} \left( \delta^{ij} - \frac{q^i q^j}{\vec{q}^2} \right) \Sigma_{ij}, \quad \Sigma_L = \frac{q^2}{q_0^2} \frac{q^i q^j}{\vec{q}^2} \Sigma_{ij}. \quad (3)$$

(In the special case  $\vec{q} = 0$  this reduces to  $\Sigma_T = \Sigma_L = \frac{1}{3} \delta^{ij} \Sigma_{ij}$ .) The angular integrations for  $\Sigma_T$  and  $\Sigma_L$  can be performed analytically. For time-like momenta,  $q^2 > 0$ , the final expressions are given e.g. in Ref. [18].

Numerical results for  $\Sigma_{\rho\pi\pi T}$  and  $\Sigma_{\rho\pi\pi L}$  are shown in Figs. 3a to 3d (solid lines). Above the two-pion threshold,  $q^2 > 4m_\pi^2$ , i.e.  $q_0 > 410$  MeV in Fig. 3,  $\Sigma_{\rho\pi\pi}$  receives an imaginary part from the first term in Eq. (2), which describes the decay into a  $\pi^+\pi^-$  pair (Fig. 2c). This imaginary part exists already in vacuum, but is Bose-enhanced by a factor  $1+2n_{\vec{k}}$  at  $T > 0$ . In the space-like region,  $q^2 < 0$ , i.e.  $q_0 < 300$  MeV in Fig. 3, also the second term in Eq. (2) generates an imaginary part in  $\Sigma_{\rho\pi\pi}$ , describing the absorption of the virtual  $\rho$ -meson by a thermal pion (Fig. 2d) and therefore vanishing in vacuum. The main reason for the completely different behavior of  $\Sigma_{\rho\pi\pi T}$  and  $\Sigma_{\rho\pi\pi L}$  in this region is the factor  $q^2/q_0^2$  in Eq. (3). The real parts of  $\Sigma_{\rho\pi\pi T}$  and  $\Sigma_{\rho\pi\pi L}$  in the time-like region are larger than the real part of  $\Sigma^{vac}$ , thus shifting the  $\rho$ -meson pole to higher energies. The main reasons for this shift are the factor  $1+2n_{\vec{k}}$  in numerator of the third term in Eq. (2) (“tadpole” graph, Fig. 2b), and the second term, which has a positive real part for  $q_0 > \vec{q}$ . In Fig. 3c, the effect of the second term can be inferred from the steep rise of  $\text{Re } \Sigma_{\rho\pi\pi T}$  in the region where this term contributes to  $\text{Im } \Sigma_{\rho\pi\pi T}$ , i.e. in the interval  $0 < q_0 < 300$  MeV.

The shift of the pole mass and the broadening of the peak due to the Bose-enhancement of  $\text{Im } \Sigma_{\rho\pi\pi}$  can be seen more clearly in the spectral functions. To calculate these at finite

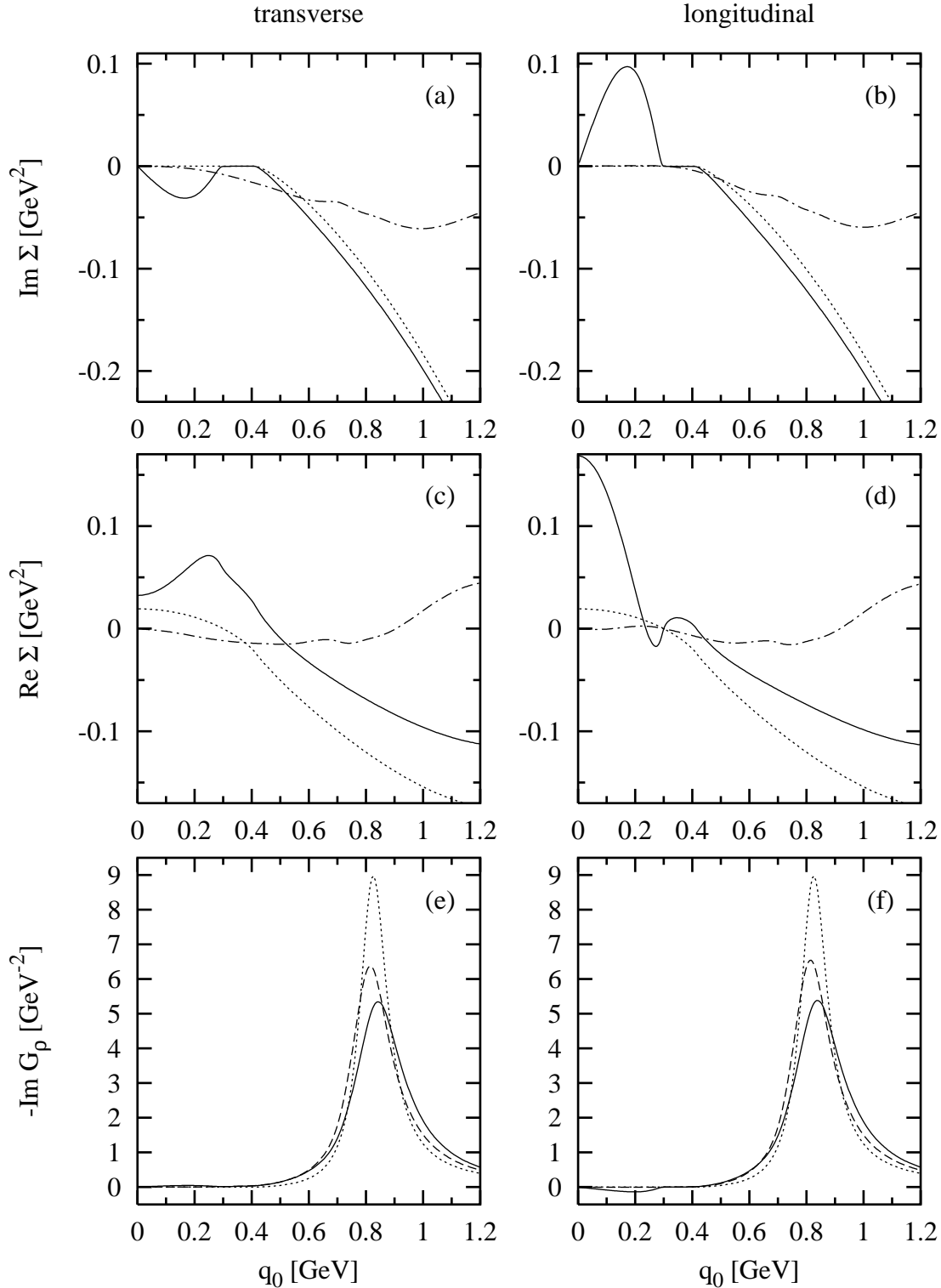


Figure 3: (a) to (d) Transverse and longitudinal  $\rho$ -meson self-energies for fixed 3-momentum  $|\vec{q}| = 300$  MeV as functions of energy  $q_0$ , without baryons ( $\rho_B = 0$ ):  $\Sigma^{vac}$  (dotted lines),  $\Sigma_{\rho\pi\pi}$  for  $T = 150$  MeV (solid lines) and  $\Sigma_{\rho M}$  for  $T = 150$  MeV (dashed-dotted lines). (e) and (f) Imaginary parts of the transverse and longitudinal  $\rho$ -meson propagators: in vacuum (dotted lines) and for  $T = 150$  MeV within the full model (solid lines) and neglecting temperature effects in  $\Sigma_{\rho\pi\pi}$  (dashed lines).

temperature, we must consider also the self-energy contribution  $\Sigma_{\rho M}$ , corresponding to diagrams like Fig. 1c. This is not the topic of this article, so we simply take the results from Ref. [19] (dashed-dotted lines in Figs. 3a to 3d). The spectral functions at finite temperature are now obtained by taking the imaginary part of

$$G_{\rho T,L}(q_0, \vec{q}) = \frac{1}{q^2 - m_\rho^{(0)2} - \Sigma_{tot T,L}}, \quad (4)$$

where  $\Sigma_{tot} = \Sigma_{\rho\pi\pi} + \Sigma_{\rho M}$ . These spectral functions are shown in Figs. 3e and 3f as the solid lines. The dashed lines have been obtained by neglecting the temperature effects in  $\Sigma_{\rho\pi\pi}$ , i.e.  $\Sigma_{tot}$  in Eq. (4) has been replaced by  $\Sigma^{vac} + \Sigma_{\rho M}$ . Therefore the difference between the dashed and the full lines is due to the temperature effects in  $\Sigma_{\rho\pi\pi}$  discussed above.

### 3 The pion in hot nuclear matter

In cold nuclear matter the interaction of the pion with the surrounding nucleons leads to a mixture of the pion with nucleon-hole ( $Nh$ ) and Delta-hole ( $\Delta h$ ) excitations. In this section we will evaluate the corresponding diagrams at finite temperature,  $T$ . As in our zero temperature calculation [15], we start from the interaction Lagrangians

$$\mathcal{L}_{\pi N} = \frac{f_{\pi NN}}{m_\pi} \bar{\psi} \gamma^5 \gamma^\mu \vec{\tau} \psi \cdot \partial_\mu \vec{\phi}, \quad \mathcal{L}_{\pi N\Delta} = -\frac{f_{\pi N\Delta}}{m_\pi} \bar{\psi} \vec{T}^\dagger \psi_\mu \cdot \partial^\mu \vec{\phi} + \text{h.c.}, \quad (5)$$

with  $f_{\pi NN}^2/(4\pi) = 0.081$  and  $f_{\pi N\Delta} = 2f_{\pi NN}$  (Chew-Low value), and expand the vertices and spinors to leading order in  $1/m_N$  or  $1/m_\Delta$  to obtain standard non-relativistic Feynman rules. In the nucleon and Delta propagators, we neglect the antiparticle contributions, but keep the relativistic kinematics,  $\omega_{N,\Delta}(\vec{p}) = \sqrt{m_{N,\Delta}^2 + \vec{p}^2}$ . (We have performed the calculations also with the non-relativistic kinematics,  $\omega_{N,\Delta}(\vec{p}) = m_{N,\Delta} + \vec{p}^2/(2m_{N,\Delta})$ , but found only very small differences in the final results for the  $\rho$ -meson self-energy.)

When calculating  $Nh$  and  $\Delta h$  excitations at finite temperature, we obtain the following generalized Lindhard functions:

$$\begin{aligned} \Pi_{Nh}(k_0, \vec{k}) &= 4 \left( \frac{f_{\pi NN}}{m_\pi} \right)^2 \int \frac{d^3 p}{(2\pi)^3} n_N(\vec{p}) \frac{2(\omega_N(\vec{p} + \vec{k}) - \omega_N(\vec{p}))}{(k_0 + i\varepsilon)^2 - (\omega_N(\vec{p} + \vec{k}) - \omega_N(\vec{p}))^2}, \quad (6) \\ \Pi_{\Delta h}(k_0, \vec{k}) &= \frac{16}{9} \left( \frac{f_{\pi N\Delta}}{m_\pi} \right)^2 \int \frac{d^3 p}{(2\pi)^3} (n_N(\vec{p}) - n_\Delta(\vec{p} + \vec{k})) \\ &\quad \times \frac{2(\omega_\Delta(\vec{p} + \vec{k}) - \omega_N(\vec{p}))}{(k_0 + \frac{i}{2}\Gamma_\Delta)^2 - (\omega_\Delta(\vec{p} + \vec{k}) - \omega_N(\vec{p}))^2}. \quad (7) \end{aligned}$$

Here we have adopted the notation  $n_{N,\Delta}(\vec{p}) = 1/(e^{(\omega_{N,\Delta}(\vec{p}) - \mu_B)/T} + 1)$ , and the nucleon and Delta densities as functions of  $T$  and the baryon chemical potential  $\mu_B$  are given by

$$\varrho_N = 4 \int \frac{d^3 p}{(2\pi)^3} n_N(\vec{p}), \quad \varrho_\Delta = 16 \int \frac{d^3 p}{(2\pi)^3} n_\Delta(\vec{p}), \quad (8)$$

i.e. in this context the Delta is treated as a stable particle. However, in the  $\Delta h$  Lindhard function  $\Pi_{\Delta h}$  (Eq. (7)), a constant Delta width  $\Gamma_\Delta$  is introduced, in such a way that  $\Pi_{\Delta h}$  has the analytic properties of a Fourier-transformed retarded function.

As described in Ref. [15], we account for the effect of the repulsive short-range  $NN$  and  $N\Delta$  interaction through phenomenological Migdal parameters  $g'$  [20], which is important to avoid pion condensation. The fact that nucleon and Delta are not elementary particles is taken into account by introducing a monopole form factor  $\Gamma_\pi(\vec{k}) = \Lambda^2/(\Lambda^2 + \vec{k}^2)$  at the  $\pi NN$  and  $\pi N\Delta$  vertices. The values of the parameters  $g'$  and  $\Lambda$  are constrained from a fit to photoabsorption cross sections [15, 16], resulting in  $g'_{11} = 0.6$ ,  $g'_{12} = g'_{22} = 0.25$  and as an upper value  $\Lambda = 550$  MeV. Now the total pion self-energy reads

$$\Pi = \Gamma_\pi^2 \frac{\Pi_{Nh} + \Pi_{\Delta h} - (g'_{11} - 2g'_{12} + g'_{22})\Pi_{Nh}\Pi_{\Delta h}}{1 - g'_{11}\Pi_{Nh} - g'_{22}\Pi_{\Delta h} + (g'_{11}g'_{22} - g'_{12}^2)\Pi_{Nh}\Pi_{\Delta h}}, \quad (9)$$

and the in-medium pion propagator is given by

$$G_\pi(k_0, \vec{k}) = \frac{1}{(k_0 + i\varepsilon)^2 - m_\pi^2 - \vec{k}^2(1 + \Pi(k_0, \vec{k}))}. \quad (10)$$

The influence of temperature on the medium modifications can be summarized as follows: For fixed baryon density  $\varrho_B$ , the nucleon density  $\varrho_N$  becomes smaller at finite temperature,  $T$ . This reduces the strength of  $Nh$  and  $\Delta h$  excitations. Furthermore, as also Delta states are occupied,  $\Delta h$  excitations become suppressed by Pauli blocking, such that the medium effects are reduced even if  $\varrho_N$  is kept constant<sup>1</sup>. Another temperature effect is the broadening of the  $Nh$  and  $\Delta h$  Lindhard functions due to thermal motion of the nucleons and Deltas. The peaked structures in the pion spectral function ( $Nh$ ,  $\pi$  and  $\Delta h$  peaks), which exist at zero temperature, become completely washed out at higher temperatures as indicated in Fig. 4.

At zero temperature the in-medium pion can be described as a mixture of three quasi-particles,  $(Nh)_L$ ,  $\pi$  and  $(\Delta h)_L$ . This so-called “three-level model” is equivalent to neglecting the Fermi motion of the nucleons. As a consequence of the temperature effects described above, it seems to be not very reasonable to construct such a model also for  $T > 0$ .

## 4 The $\rho$ -meson in hot nuclear matter

It has been shown by several authors [7, 8, 9], that simply replacing the free pion propagators in the  $\rho$ -meson self-energy  $\Sigma_{\rho\pi\pi}$  (Figs. 2a and 2b) by in-medium ones violates gauge invariance and leads to a strong overestimation of the medium modifications. To preserve gauge invariance, corrections to the  $\rho\pi\pi$  and  $\rho\rho\pi\pi$  vertices must be taken into account, which are related to the pion self-energy through Ward-Takahashi identities. For illustration, some of the vertex corrections related to the  $Nh$  pion self-energy contribution are shown in Fig. 5. Neglecting the anomalous magnetic moments of the nucleons, the

<sup>1</sup> In reality these two effects might be less important, because the role of the suppressed  $Nh = NN^{-1}$  and  $\Delta h = \Delta N^{-1}$  excitations is partly taken over by  $B_1^*B_1^{*-1}$  and  $B_2^*B_1^{*-1}$  excitations [14], where  $B_1^*$  and  $B_2^*$  denote any baryon resonances ( $\Delta(1232)$ ,  $N^*(1520)$  etc.). Unfortunately most of the  $\pi B_1^*B_1^*$  and  $\pi B_1^*B_2^*$  coupling constants are not well known. For  $B_2^*B_1^{*-1}$  excitations with quantum numbers of a  $\rho$ -meson (“rhosobars”) it has been found that the inclusion of higher resonances reduces the suppression effects by  $\approx 40\%$  [14], but does not compensate them.

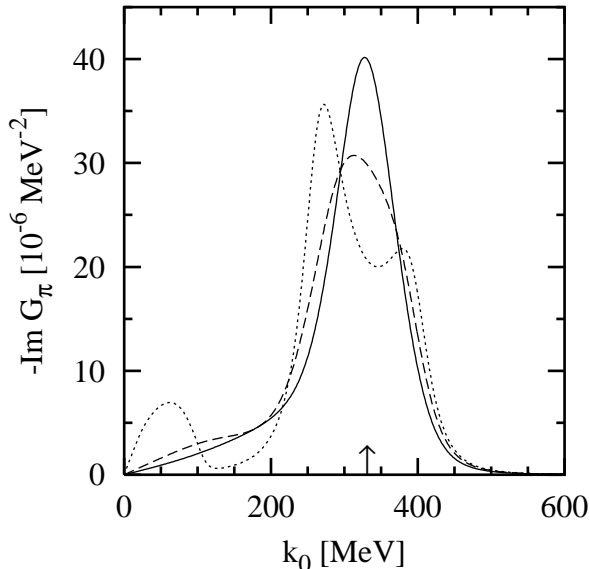


Figure 4: Imaginary part of the in-medium pion propagator for fixed 3-momentum  $|\vec{k}| = 300$  MeV as a function of energy  $k_0$ , for  $\varrho_N = 0.55\varrho_0 = 0.088$  fm $^{-3}$  and various temperatures:  $T = 0$  ( $\mu_B = 963$  MeV, dotted line),  $T = 80$  MeV ( $\mu_B = 766$  MeV, dashed line) and  $T = 150$  MeV ( $\mu_B = 452$  MeV, solid line). For comparison, the arrow indicates the pole position of a free pion ( $k_0 \approx 331$  MeV).

$\rho NN$  and  $\rho\pi NN$  couplings can be derived by minimal substitution in the free nucleon Lagrangian  $\mathcal{L}_N$  and the  $\pi N$  interaction Lagrangian  $\mathcal{L}_{\pi N}$ :

$$\mathcal{L}_{\rho N} = -\frac{g}{2}\bar{\psi}\boldsymbol{\rho}\boldsymbol{\tau}_3\psi, \quad \mathcal{L}_{\rho\pi N} = ig\frac{f_{\pi NN}}{m_\pi}\bar{\psi}\boldsymbol{\gamma}^5\boldsymbol{\rho}\vec{\tau}\psi \cdot T_3\vec{\phi}. \quad (11)$$

In Ref. [15] we have shown that the leading term in a non-relativistic expansion of the  $\rho NN$  interaction is the coupling of the  $\rho$ -meson to the nucleon charge, contributing only to the time component of the  $\rho NN$  vertex. The spatial components are of the order  $1/m_N$ . If we neglect them, only the diagrams shown in Figs. 5a and 5c are relevant for the spatial components of the  $\rho$ -meson self-energy<sup>2</sup>. For the  $\Delta h$  part, similar vertex corrections must be calculated. This can be done in analogy to the  $Nh$  part described above. The Migdal parameters  $g'$  correspond to an iteration of the  $Nh$  and  $\Delta h$  bubbles and therefore lead to additional vertex corrections. Because of the monopole form factor  $\Gamma_\pi$  at the  $\pi NN$  and  $\pi N\Delta$  vertices, the  $\rho\pi NN$  and  $\rho\pi N\Delta$  vertices must be modified in a non-trivial way [9, 21] as has been described in detail in Ref. [15].

With these vertex corrections the spatial components of the pion cloud contribution to the  $\rho$ -meson self-energy,  $\Sigma_{ij}$  (we omit the index “ $\rho\pi\pi$ ” in the following paragraphs), become a sum of seven terms, corresponding to the seven classes of diagrams shown in Fig. 6. The diagrams 6a and 6e are the same as in vacuum (Figs. 2a and 2b), but with

<sup>2</sup> Within a slightly simplified model (zero temperature, 2-level model for the pion without Migdal parameter  $g'$ ), we have performed the full calculation also allowing for  $\rho$ -meson coupling to the convection current. For time-like momenta,  $q^2 > 0$ , which are relevant for dilepton spectra, the effect of these terms is small, but, as expected, in the space-like region near the quasi-elastic peak, the approximation becomes quite bad.



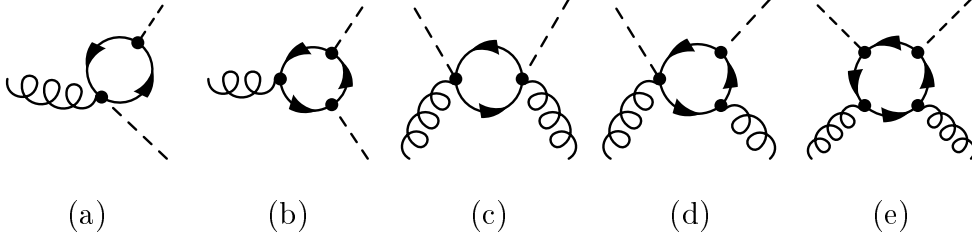


Figure 5: Some of the  $\rho\pi\pi$  and  $\rho\rho\pi\pi$  vertex correction diagrams corresponding to the  $Nh$  pion self-energy.

the bare pion propagators replaced by in-medium ones. The diagrams 6b to 6d and 6f to 6g are obtained by including  $\rho\pi\pi$  vertex corrections in diagram 6a and  $\rho\rho\pi\pi$  vertex corrections in diagram 6d, respectively. The diagrams 6a to 6d and 6f can be cut into two parts, i.e. they depend on  $q_0$  and  $\vec{q}$  and contribute to both the real and imaginary parts of  $\Sigma_{ij}$ . The diagrams 6e and 6g cannot be cut and are therefore real and  $q_0$ -independent. However, because of the coupling of the  $\rho$ -meson to the  $\pi NN$  and  $\pi N\Delta$  monopole form factor in diagram 6g, their contribution still depends on the 3-momentum  $\vec{q}$ .

Let us first look at these purely real and energy independent (“constant”) contributions. Their sum,  $\Sigma_{ij}^C$ , has the structure

$$\Sigma_{ij}^C(\vec{q}) = g^2 \int \frac{d^3k}{(2\pi)^3} \sum_{r=5,7} f_{ij}^{(r)}(\vec{q}, \vec{k}) J_r(\vec{k}) . \quad (12)$$

The  $r = 5$  and  $r = 7$  terms correspond to the diagrams 6e and 6g, respectively. Explicit expressions for the functions  $f_{ij}^{(r)}$ , which are simple combinations of  $\vec{q}$ ,  $\vec{k}$  and  $\Lambda$ , are given in the appendix. The functions  $J_5$  and  $J_7$  are defined as sums over Matsubara frequencies  $\omega_m = \pi mT$ :

$$J_5(\vec{k}) = -2T \sum_{m \text{ even}} \mathcal{G}_\pi(\omega_m, \vec{k}) , \quad J_7(\vec{k}) = -2T \sum_{m \text{ even}} \mathcal{J}(\omega_m, \vec{k}) \mathcal{G}_\pi(\omega_m, \vec{k}) . \quad (13)$$

Here  $\mathcal{G}_\pi(\omega_m, \vec{k})$  denotes the imaginary-time pion propagator, which is related to the retarded propagator  $G_\pi$  by its Lehmann representation [17],

$$\mathcal{G}_\pi(\omega_m, \vec{k}) = -\frac{1}{\pi} \int d\omega \frac{\text{Im} G_\pi(\omega, \vec{k})}{i\omega_m - \omega} . \quad (14)$$

In an analogous way  $\mathcal{J}(\omega_m, \vec{k})$  is related to the retarded pion self-energy  $\Pi$ . Inserting this into Eq. (13) and using the identity

$$-T \lim_{\eta \rightarrow 0} \sum_{m \text{ even}} \frac{e^{i\omega_m \eta}}{i\omega_m - \omega} = \frac{1}{e^{\omega/T} - 1} =: f(\omega) , \quad (15)$$

we can evaluate the sum over  $\omega_m$ , with the result

$$J_5(\vec{k}) = -\frac{2}{\pi} \int_0^\infty d\omega \left(1 + 2f(\omega)\right) \text{Im} G_\pi(\omega, \vec{k}) \quad (16)$$

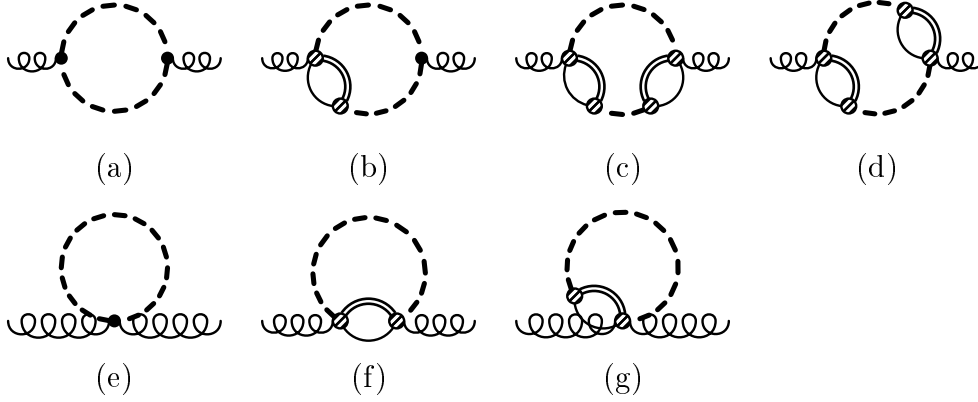


Figure 6: Feynman diagrams for the spatial components of the pion cloud contribution to the  $\rho$ -meson self-energy in hot hadronic matter. The thick dashed lines represent in-medium pion propagators, the bubbles represent the total pion self-energy with the  $\pi NN$  or  $\pi N\Delta$  monopole form factors indicated by the hatched blobs.

and a similar expression for  $J_7$ .

Next we turn to the energy-dependent part of  $\Sigma_{ij}$ , represented by the diagrams 6a to 6d and 6f. It has the structure

$$\Sigma_{ij}(q_0, \vec{q}) - \Sigma_{ij}^C(\vec{q}) = g^2 \int \frac{d^3k}{(2\pi)^3} \sum_{r=1,2,3,4,6} f_{ij}^{(r)}(\vec{q}, \vec{k}) I_r(q_0, \vec{q}, \vec{k}). \quad (17)$$

The  $r = 1$ ,  $r = 2$  and  $r = 4$  terms correspond directly to the diagrams 6a, 6b and 6d, whereas the definitions of the  $r = 3$  and  $r = 6$  terms are somewhat more complicated: The pion self-energy bubble in diagram 6f can be separated into a spin-longitudinal and a spin-transverse part. The  $r = 6$  term contains only the transverse part, whereas the longitudinal part is combined with diagram 6c in the  $r = 3$  term.

Note that the entire  $q_0$  dependence is contained in the functions  $I_r$ . These are obtained by analytical continuation of functions  $J_r$ , which originally are defined only for discrete Matsubara frequencies  $\omega_n$ ,  $n$  even:

$$I_r(q_0, \vec{q}, \vec{k}) = J_r(\omega_n \rightarrow -i(q_0 + i\varepsilon), \vec{q}, \vec{k}). \quad (18)$$

For example, the function  $J_1$  is defined as follows:

$$J_1(\omega_n, \vec{q}, \vec{k}) = -2T \sum_{m \text{ even}} \mathcal{G}_\pi(\omega_m, \vec{k}) \mathcal{G}_\pi(\omega_{m+n}, \vec{k} + \vec{q}). \quad (19)$$

The definitions of the other functions  $J_r$  are listed in the appendix.

As described already for  $J_5$ , we insert the Lehmann representation of  $\mathcal{G}_\pi$  into Eq. (19) and evaluate the sum over  $\omega_m$  by using Eq. (15). After these steps the analytical continuation of  $J_1$  to  $I_1$  reduces to a simple replacement according to Eq. (18). For the imaginary part we obtain

$$\begin{aligned} \text{Im } I_1(q_0, \vec{q}, \vec{k}) &= -\frac{2}{\pi} \int_0^{q_0} d\omega \left( 1 + f(\omega) + f(q_0 - \omega) \right) \\ &\quad \times \text{Im } G_\pi(\omega, \vec{k}) \text{Im } G_\pi(q_0 - \omega, \vec{k} + \vec{q}) \end{aligned}$$

$$\begin{aligned}
& -\frac{2}{\pi} \int_0^\infty d\omega \left( f(\omega) - f(q_0 + \omega) \right) \\
& \quad \times \left( \text{Im } G_\pi(\omega, \vec{k}) \text{Im } G_\pi(q_0 + \omega, \vec{k} + \vec{q}) \right. \\
& \quad \left. + \text{Im } G_\pi(q_0 + \omega, \vec{k}) \text{Im } G_\pi(\omega, \vec{k} + \vec{q}) \right). \quad (20)
\end{aligned}$$

In the same way we derive similar expressions for the imaginary parts of the remaining functions  $I_2$  to  $I_4$  and  $I_6$ . Rather than by direct calculation, the real part of the energy-dependent piece of the  $\rho$ -meson self-energy,  $\Sigma_{ij} - \Sigma_{ij}^C$ , can be computed more efficiently from the imaginary part using a dispersion relation. The convergence of the dispersion integral is improved by subtracting the vacuum contribution:

$$\text{Re } \Sigma_{ij}(q_0, \vec{q}) = \text{Re } \Sigma_{ij}^{vac}(q_0, \vec{q}) + \Sigma_{ij}^{C\ med}(\vec{q}) - \frac{1}{\pi} \mathcal{P} \int_0^\infty d\omega^2 \frac{\text{Im } \Sigma_{ij}^{med}(\omega, \vec{q})}{q_0^2 - \omega^2}. \quad (21)$$

Figs. 7a to 7d display numerical results for the  $\rho$ -meson self-energy in a baryonic medium with  $\varrho_N = 0.55\varrho_0$ . Because of the approximations employed for the  $\rho NN$  vertex, we restrict ourselves to  $q^2 > 0$  (see footnote on page 8) and plot the results as functions of the invariant mass  $M = \sqrt{q^2}$ .

Let us first discuss the imaginary part of the self-energy (Figs. 7a and 7b). The dashed lines show the transverse and longitudinal parts of  $\Sigma_{\rho\pi\pi}$  for  $\varrho_N = 0.55\varrho_0$  and  $T = 0$ . Compared with  $\Sigma^{vac}$  (dotted lines), the following medium modifications are visible: The threshold disappears, because the  $\rho$ -meson can “decay” into two  $Nh$  excitations. The steep rise of  $\text{Im } \Sigma_{\rho\pi\pi}$  at  $M \approx 400$  MeV and the large imaginary part above this energy is mainly a result of the “decay” of the  $\rho$ -meson into a pion and a transverse  $\Delta h$  excitation ( $r = 6$  term, diagram 6f). A more detailed discussion of these effects can be found in Ref. [15].

The solid lines show  $\Sigma_{\rho\pi\pi}$  for  $T = 150$  MeV. For a discussion of the differences to the  $T = 0$  case, consider e.g. Eq. (20), which describes the imaginary part of the  $r = 1$  term. At higher energies ( $M \gtrsim 300$  MeV) the imaginary part is dominated by the first integral, which contributes already at  $T = 0$ , but is enhanced at  $T > 0$  by the Bose-factor  $1 + f(\omega) + f(q_0 - \omega)$ . It describes the “decay” of the  $\rho$ -meson into two in-medium pions with energies  $\omega$  and  $q_0 - \omega$  (Fig. 2c with the free pions replaced by in-medium ones:  $\rho \rightarrow \pi_{med} + \pi_{med}$ , including processes such as  $\rho \rightarrow Nh + \pi$ ,  $\rho \rightarrow \Delta h + \pi$  etc.). At very low energies ( $M \lesssim 200$  MeV), the second integral in Eq. (20) is more important. It exists only at  $T > 0$  because of the factor  $f(\omega) - f(q_0 + \omega)$ . Therefore  $\text{Im } \Sigma_{\rho\pi\pi}$  increases strongly with temperature in this low-energy region. The corresponding physical process is the “absorption” of the  $\rho$ -meson by a thermal pion with energy  $\omega$ , giving the outgoing pion the energy  $q_0 + \omega$  (Fig. 2d with the free pions replaced by in-medium ones:  $\rho + \pi_{med} \rightarrow \pi_{med}$ ). In the absence of baryons,  $\varrho_B = 0$ , this is possible only for space-like 4-momenta,  $q^2 < 0$ , i.e. for  $q_0 < |\vec{q}|$  (see Section 2). At finite baryon density the situation changes, however, as a consequence of the broadening of the pion spectral function, such that this term contributes also for  $q^2 > 0$  (e.g. via the process  $\rho + \pi \rightarrow \Delta h$ , which is of course contained in the class of processes  $\rho + \pi_{med} \rightarrow \pi_{med}$ .)

Finally, the dashed-dotted curves represent the sum of the remaining self-energy contributions,  $\Sigma_{\rho B} + \Sigma_{\rho M}$ , for  $T = 150$  MeV and  $\varrho_N = 0.55\varrho_0$ . The contribution  $\Sigma_{\rho M}$  has been considered already in Section 2, we have taken it from Ref. [19] and displayed it in Fig. 3.

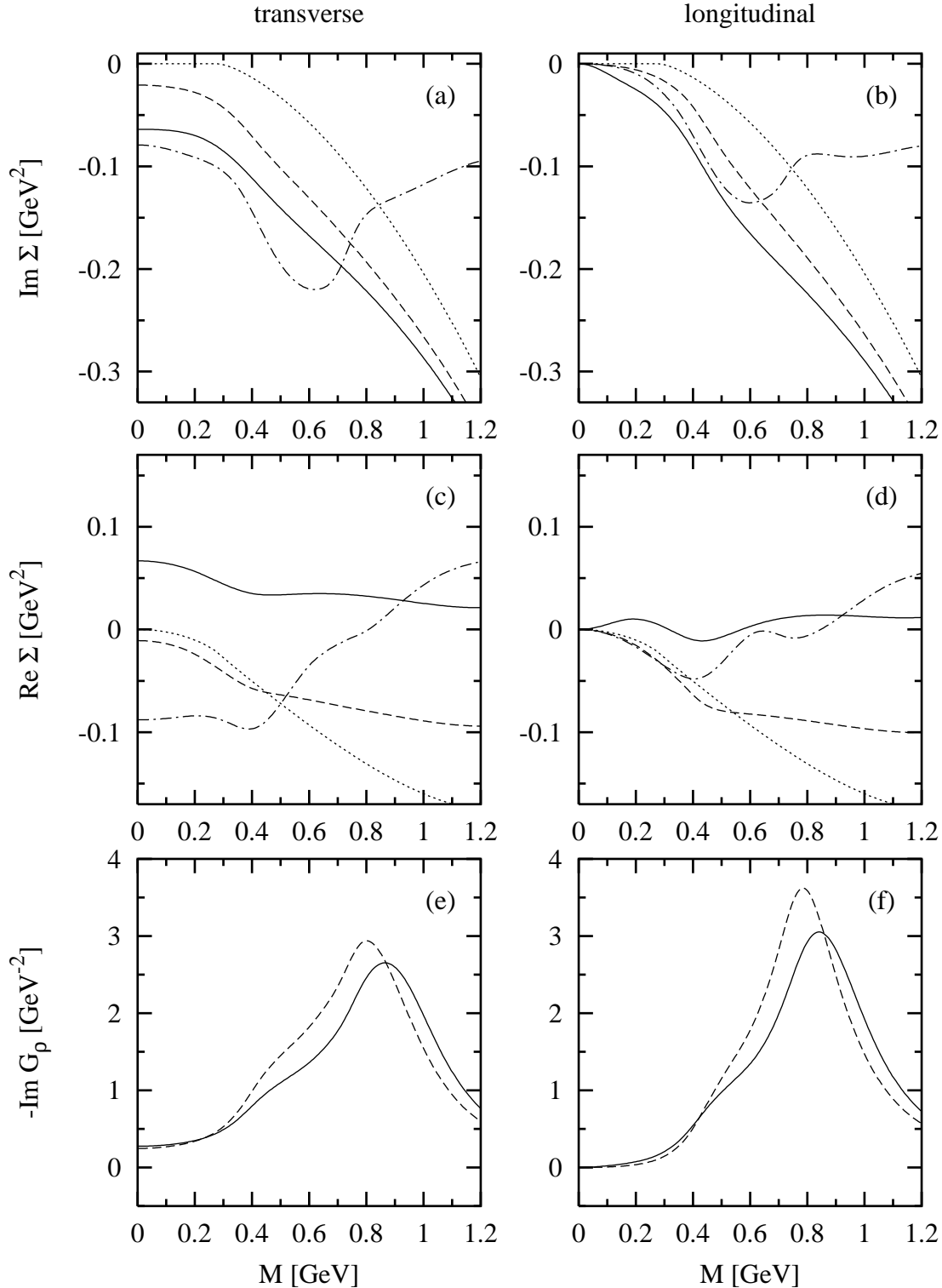


Figure 7: (a) to (d) Transverse and longitudinal  $\rho$ -meson self-energies for fixed 3-momentum  $|\vec{q}| = 300$  MeV as functions of the invariant mass  $M$  in vacuum (dotted lines) and for  $\varrho_N = 0.55\varrho_0 = 0.088$  fm $^{-3}$ :  $\Sigma_{\rho\pi\pi}$  for  $T = 0$  ( $\mu_B = 963$  MeV, dashed lines),  $\Sigma_{\rho\pi\pi}$  for  $T = 150$  MeV ( $\mu_B = 452$  MeV, solid lines) and  $\Sigma_{\rho B} + \Sigma_{\rho M}$  for  $T = 150$  MeV (dashed-dotted lines). (e) and (f)  $\rho$ -meson spectral functions for  $\varrho_N = 0.55\varrho_0 = 0.088$  fm $^{-3}$  and  $T = 150$  MeV within the full model (solid lines) and neglecting temperature effects in  $\Sigma_{\rho\pi\pi}$  (dashed lines).

The contribution  $\Sigma_{\rho B}$  corresponds to diagrams as shown in Fig. 1b. It is described in Ref. [16] for  $T = 0$  and has been extended to finite temperature [13, 14]. The parameters of the model have been fixed by fitting  $B \rightarrow \rho N$  decay widths and photoabsorption cross sections of the nucleon and of nuclei [16]. (Note that in Ref. [14] the photoabsorption cross-section is fitted with a very soft  $\pi NN$  form factor,  $\Lambda = 300$  MeV, while we take  $\Lambda = 550$  MeV as in Ref. [16]. Therefore in Ref. [14]  $\Sigma_{\rho B}$  is larger and  $\Sigma_{\rho\pi\pi}$  is smaller than in this article.)

Let us now turn to the real part of the self-energy (Figs. 7c and 7d). Comparing the dotted, dashed and solid curves, we find that both, density and temperature, increase  $\text{Re}\Sigma_{\rho\pi\pi}$  in the region of the  $\rho$ -meson pole, shifting it to higher energies. For the case  $\varrho_B = 0$  we have noted this temperature effect already in Section 2 (Fig. 3). It is caused mainly by  $\Sigma^C$  (factor  $1 + 2f(\omega)$  in Eq. (16)) and by the energy-dependent real parts related to the second integral in Eq. (20). Contrary to  $\text{Re}\Sigma_{\rho\pi\pi}$ , the real part of  $\Sigma_{\rho B} + \Sigma_{\rho M}$  (dashed-dotted lines) is almost zero at  $M \approx 800$  MeV and therefore does not shift the position of the pole.

The medium effects can be seen more clearly in the spectral functions than in the self-energies. They are displayed in Figs. 7e and 7f. The solid lines represent the full calculation for  $T = 150$  MeV and  $\varrho_N = 0.55\varrho_0$ , i.e. using Eq. (4) with  $\Sigma_{tot} = \Sigma_{\rho\pi\pi} + \Sigma_{\rho B} + \Sigma_{\rho M}$ . As we expected already from the discussion of the self-energies, the width of the  $\rho$ -meson is strongly increased compared with the vacuum, and the pole mass, i.e. the position of the maximum, is shifted upwards from 770 MeV in vacuum to 865 MeV for  $\text{Im}G_{\rho T}$  and to 840 MeV for  $\text{Im}G_{\rho L}$ , respectively. Since we are mainly interested in the temperature effects in  $\Sigma_{\rho\pi\pi}$ , we show as the dashed curve a spectral function that has been obtained by neglecting these temperature effects, i.e.  $\Sigma_{tot}$  has been replaced by  $\Sigma_{\rho\pi\pi}(T = 0) + \Sigma_{\rho B} + \Sigma_{\rho M}$ . Now one can see clearly that about 70% of the total mass shift is due to the temperature effects in  $\Sigma_{\rho\pi\pi}$ .

## 5 Dilepton and photon rates

Our main motivation for the investigation of the  $\rho$ -meson in hot and dense matter is the description of dilepton production in heavy-ion collisions. Assuming hadronic matter in (local) thermal and chemical equilibrium (temperature  $T$ , baryon chemical potential  $\mu_B$ ) and Sakurai's vector dominance model (VDM) [2], the production rate ( $R = dN/d^4x$ ) of  $e^+e^-$  pairs with 4-momentum  $q$  in the low invariant mass region ( $M = \sqrt{q^2} < 1$  GeV) in the isovector ( $\rho$ -meson) channel is given by [8]

$$\frac{dR_{e^+e^-}}{d^4q} = \frac{\alpha^2}{3\pi^3 q^2} \frac{1}{e^{q_0/T} - 1} \frac{m_\rho^{(0)4}}{g^2} g_{\mu\nu} \text{Im} G_\rho^{\mu\nu}(q_0, \vec{q}; \mu_B, T), \quad (22)$$

where  $\alpha = e^2/(4\pi) = 1/137$ . In the derivation of this expression the electron mass has been neglected. However, if one includes the baryonic contribution  $\Sigma_{\rho B}$ , it is necessary to formulate the VDM such that the  $\rho NB$  and  $\gamma NB$  couplings can be adjusted independently [3, 10]. Then the expression  $m_\rho^{(0)4}/g^2 g_{\mu\nu} \text{Im} G_\rho^{\mu\nu}$  in Eq. (22) is replaced by [14]

$$\frac{m_\rho^{(0)4}}{g^2} g_{\mu\nu} \text{Im} G_\rho^{\mu\nu} \rightarrow \frac{1}{g^2} (2F_T + F_L), \quad (23)$$

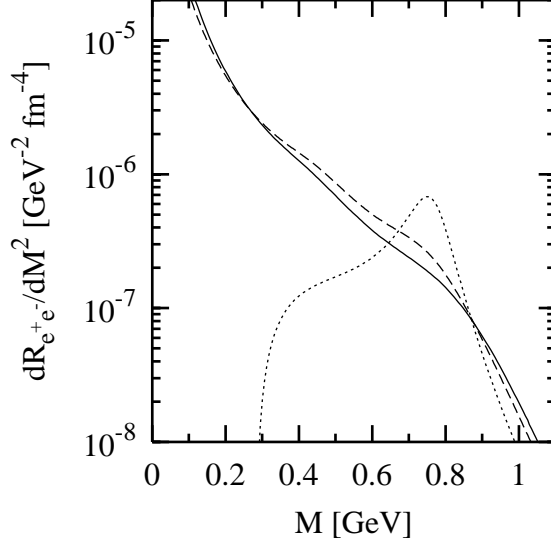


Figure 8: Dilepton production rate  $dR_{e^+e^-}/dM^2$  for  $T = 150$  MeV obtained without medium modifications of the  $\rho$ -meson (dotted line) and with medium modifications for  $\varrho_N = 0.55\varrho_0$ : full model (solid line) and neglecting temperature effects in  $\Sigma_{\rho\pi\pi}$  (dashed line).

where

$$F_L = -m_\rho^{(0)4} \text{Im} G_{\rho L} , \quad (24)$$

$$F_T = -(\text{Im} \Sigma_{\rho\pi\pi T} + \text{Im} \Sigma_{\rho M T}) |d_\rho - 1| - \text{Im} \Sigma_{\rho B T} |d_\rho - r_B| , \quad (25)$$

$$d_\rho = (q^2 - \Sigma_{\rho\pi\pi T} - \Sigma_{\rho M T} - r_B \Sigma_{\rho B T}) G_{\rho T} . \quad (26)$$

The parameter  $r_B = 0.7$  [16] is the ratio of the actual  $\gamma NB$  coupling to the  $\gamma NB$  coupling derived in Sakurai's VDM.

Results for the dilepton rate as a function of  $M$ , i.e. integrated over  $\vec{q}$ , are displayed in Fig. 8 for  $T = 150$  MeV and  $\varrho_N = 0.55\varrho_0$ , corresponding to conditions as expected to be realized in the  $E_{lab} = 40$  AGeV run at the CERN-SpS. Without any medium modifications of the  $\rho$ -meson, the dilepton rate is peaked around  $M = 770$  MeV (dotted line). With medium modifications, the peak disappears and the dilepton rate for  $M \lesssim 650$  MeV is strongly enhanced (solid line). If one neglects temperature effects in  $\Sigma_{\rho\pi\pi}$  (dashed line), the rate in this region is slightly overestimated (by 15% at  $M = 400$  MeV) because of the  $\rho$ -meson mass shift observed in Section 4. The difference is even larger at  $M \approx 770$  MeV, where the full result (solid line) is 30% below the result obtained by neglecting temperature effects in  $\Sigma_{\rho\pi\pi}$  (dashed line). Therefore the temperature effects in  $\Sigma_{\rho\pi\pi}$ , principally the mass shift, might improve the description of the experimental dilepton spectra which, in this invariant mass region, are almost saturated by  $e^+e^-$ -pairs expected from free  $\omega$ -meson decays after freeze-out.

Besides dilepton pairs, also direct real photons (i.e. real photons produced inside the fireball) can be used as probes for the hot and dense phase of the fireball in heavy-ion experiments. If we make the same assumptions as in the derivation of Eq. (22), the rate for direct real photon emission is given by [22]

$$q_0 \frac{dR_\gamma}{d^3q} = \frac{\alpha}{2\pi^2} \frac{1}{e^{q_0/T} - 1} \frac{m_\rho^{(0)4}}{g^2} g_{\mu\nu} \text{Im} G_\rho^{\mu\nu}(q_0, \vec{q}; \mu_B, T) , \quad (27)$$

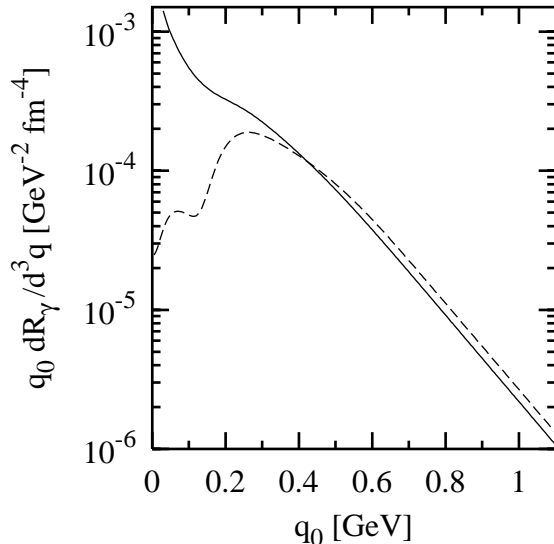


Figure 9: Direct photon production rate  $q_0 dR_\gamma/d^3q$  for  $\varrho_N = 0.55\varrho_0$  and  $T = 150$  MeV within the full model (solid line) and neglecting temperature effects in  $\Sigma_{\rho\pi\pi}$  (dashed line).

where  $q_0 = |\vec{q}|$  is the energy of a photon with momentum  $\vec{q}$ . Again, when  $\Sigma_{\rho B}$  is included, the term  $m_\rho^{(0)4}/g^2 g_{\mu\nu} \text{Im} G_\rho^{\mu\nu}$  must be replaced according to Eq. (23), but since  $F_L$  vanishes for  $q^2 = 0$ , only the transverse part  $F_T$  contributes.

Numerical results are shown in Fig. 9. Again the solid line represents the full calculation, while for the dashed line the temperature dependence of  $\Sigma_{\rho\pi\pi}$  for fixed  $\varrho_N$  has been neglected. The enhancement of the solid curve below 300 MeV is a consequence of the imaginary part of the “absorption” terms discussed at the end of Section 4, which in the context of photon emission correspond to processes such as  $\pi_{med} \rightarrow \pi_{med} + \rho \rightarrow \pi_{med} + \gamma$ , e.g.  $\Delta h \rightarrow \pi + \rho \rightarrow \pi + \gamma$ .

## 6 Summary and conclusions

In a previous article [15] we have extended the models from Refs. [8, 9], describing the modifications of the  $\rho$ -meson through the in-medium pion propagator in cold nuclear matter, i.e. through the self-energy  $\Sigma_{\rho\pi\pi}$ , to finite 3-momentum of the  $\rho$ -meson. In the present work we have also included finite-temperature effects by evaluating both, the pion and  $\rho$ -meson self-energy diagrams within the imaginary-time formalism. We stress that this is the first consistent finite-temperature calculation of  $\Sigma_{\rho\pi\pi}$ , whereas the medium modifications through resonant  $\rho$ -meson scattering off baryons ( $\Sigma_{\rho B}$ ) or mesons ( $\Sigma_{\rho M}$ ) at  $T > 0$  have already been evaluated in Refs. [13, 14, 19].

Already at moderate nucleon densities,  $\varrho_N = 0.55\varrho_0$ , the self-energy contribution  $\Sigma_{\rho\pi\pi}$  leads to significant changes of the  $\rho$ -meson spectral function. Let us summarize the most important effects: First, the width of the  $\rho$ -meson is increased. Second, the maximum of the  $\rho$ -meson spectral function, i.e. the  $\rho$ -meson “mass”, is shifted upwards in the medium. Of course, the other contributions,  $\Sigma_{\rho B}$  and  $\Sigma_{\rho M}$ , result in an additional broadening of the spectral function, but they produce almost no mass shift. Concentrating on the medium modifications through  $\Sigma_{\rho\pi\pi}$ , the  $\rho$ -meson width and mass increase with both, density and

temperature. However, the broadening depends predominantly on the density, whereas the mass shift is mainly a temperature effect.

The broadening of the spectral function results in a strong enhancement of the dilepton production rate for invariant masses below  $\approx 650$  MeV, while the peak at 770 MeV, which one would expect in a naive model (without medium modifications of the  $\rho$ -meson), disappears. The mass shift from the temperature effects in  $\Sigma_{\rho\pi\pi}$  helps to suppress the dilepton rate around 770 MeV further, but also reduces the enhancement below 650 MeV from the broadening a little. However, the results shown in Sect. 5 might be quantitatively somewhat modified if one applies the soft  $\pi NN$  form factor of  $\Lambda = 300$  MeV, as in Ref. [14], instead of  $\Lambda = 550$  MeV.

In some respects the model could be further improved. First, for the description of the pion in nuclear matter also higher resonances beyond the  $\Delta(1232)$  should be included (see footnote on page 7). Second, for the case  $T > 0$  but  $\varrho_B = 0$ , it has been shown that in a consistent treatment of  $\rho$ - and  $a_1$ -mesons, respecting chiral symmetry, the leading temperature effect essentially consists of a mixing of vector and axial-vector correlators, i.e.  $\rho$ - and  $a_1$ -meson propagators [23]. To relate the measured dilepton spectra to potential signals of chiral symmetry restoration, it is furthermore mandatory to study the medium modifications of  $\rho$ - and  $a_1$ -mesons within a chiral symmetric model also at  $\varrho_B \neq 0$ . Work in this direction is in progress.

## Acknowledgements

This work was supported in part by GSI, BMBF and NSF grant NSFPHY98-00978. One of us (RR) is supported by DOE grant no. DE-FG02-88ER40388 and is grateful for the hospitality at TU Darmstadt.

## A Explicit expressions and definitions

In Section 4 only the structure of the formula for the spatial components of the  $\rho$ -meson self-energy  $\Sigma_{\rho\pi\pi} \equiv \Sigma$  has been given (Eqs. (12) and (17)). The explicit expression reads

$$\begin{aligned}
\Sigma_{ij}(q_0, \vec{q}) &= \frac{g^2}{4} \int \frac{d^3k}{(2\pi)^3} \left( (2k+q)_i (2k+q)_j I_1(q_0, \vec{q}, \vec{k}) \right. \\
&+ 4 \frac{(k_i(\Lambda^2 - \vec{k}^2) - q_i \vec{k}^2)(2k+q)_j}{\Lambda^2 + (\vec{k} + \vec{q})^2} I_2(q_0, \vec{q}, \vec{k}) \\
&+ 2 \frac{(k_i(\Lambda^2 - \vec{k}^2) - q_i \vec{k}^2)(k_j(\Lambda^2 - \vec{k}^2) - q_j \vec{k}^2)}{\vec{k}^2(\Lambda^2 + (\vec{k} + \vec{q})^2)^2} I_3(q_0, \vec{q}, \vec{k}) \\
&+ 2 \frac{(k_i(\Lambda^2 - \vec{k}^2) - q_i \vec{k}^2)(k_j(\Lambda^2 - (\vec{k} + \vec{q})^2) + q_j \Lambda^2)}{(\Lambda^2 + (\vec{k} + \vec{q})^2)(\Lambda^2 + \vec{k}^2)} I_4(q_0, \vec{q}, \vec{k}) \\
&\left. + 2\delta_{ij} J_5(\vec{k}) \right)
\end{aligned}$$



$$\begin{aligned}
& +2 \frac{(\Lambda^2 + \vec{k}^2)^2}{(\Lambda^2 + (\vec{k} + \vec{q})^2)^2} \left( \delta_{ij} - \frac{k_i k_j}{\vec{k}^2} \right) I_6(q_0, \vec{q}, \vec{k}) \\
& -4 \left( \frac{\vec{k}^2 \delta_{ij}}{\Lambda^2 + \vec{k}^2} + \frac{(2k + q)_i (k_j (\Lambda^2 - \vec{k}^2) - q_j \vec{k}^2)}{(\Lambda^2 + (\vec{k} + \vec{q})^2) (\Lambda^2 + \vec{k}^2)} \right) J_7(\vec{k}) \\
& + (i \longleftrightarrow j) .
\end{aligned} \tag{28}$$

The retarded functions  $I_r$  are given by analytical continuation of the corresponding imaginary-time functions  $J_r$  to the real axis according to Eq. (18). The functions  $J_1$  to  $J_7$  are defined as follows:

$$J_1(\omega_n, \vec{q}, \vec{k}) = -2T \sum_{m \text{ even}} \mathcal{G}_\pi(\omega_m, \vec{k}) \mathcal{G}_\pi(\omega_{m+n}, \vec{k} + \vec{q}) , \tag{29}$$

$$J_2(\omega_n, \vec{q}, \vec{k}) = -2T \sum_{m \text{ even}} \mathbb{I}(\omega_m, \vec{k}) \mathcal{G}_\pi(\omega_m, \vec{k}) \mathcal{G}_\pi(\omega_{m+n}, \vec{k} + \vec{q}) , \tag{30}$$

$$J_3(\omega_n, \vec{q}, \vec{k}) = -2T \sum_{m \text{ even}} \mathbb{I}_L(\omega_m, \vec{k}) \mathcal{G}_\pi(\omega_{m+n}, \vec{k} + \vec{q}) , \tag{31}$$

$$\begin{aligned}
J_4(\omega_n, \vec{q}, \vec{k}) &= -2T \sum_{m \text{ even}} \mathbb{I}(\omega_m, \vec{k}) \mathcal{G}_\pi(\omega_m, \vec{k}) \\
&\quad \times \mathbb{I}(\omega_{m+n}, \vec{k} + \vec{q}) \mathcal{G}_\pi(\omega_{m+n}, \vec{k} + \vec{q}) ,
\end{aligned} \tag{32}$$

$$J_5(\vec{k}) = -2T \sum_{m \text{ even}} \mathcal{G}_\pi(\omega_m, \vec{k}) , \tag{33}$$

$$J_6(\omega_n, \vec{q}, \vec{k}) = -2T \sum_{m \text{ even}} \mathbb{I}(\omega_m, \vec{k}) \mathcal{G}_\pi(\omega_{m+n}, \vec{k} + \vec{q}) , \tag{34}$$

$$J_7(\vec{k}) = -2T \sum_{m \text{ even}} \mathbb{I}(\omega_m, \vec{k}) \mathcal{G}_\pi(\omega_m, \vec{k}) . \tag{35}$$

The imaginary-time pion self-energy  $\mathbb{I}$  and propagator  $\mathcal{G}_\pi$  are related to the corresponding retarded functions  $\Pi$  and  $G_\pi$  by their Lehmann representations

$$\mathbb{I}(\omega_m, \vec{k}) = -\frac{1}{\pi} \int d\omega \frac{\text{Im } \Pi(\omega, \vec{k})}{i\omega_m - \omega} , \quad \mathcal{G}_\pi(\omega_m, \vec{k}) = -\frac{1}{\pi} \int d\omega \frac{\text{Im } G_\pi(\omega, \vec{k})}{i\omega_m - \omega} . \tag{36}$$

As a consequence, such representations exist also for  $\mathbb{I} \mathcal{G}_\pi$  and  $\mathbb{I}_L$ , which are combinations of these functions. The longitudinal spin-isospin response function  $\Pi_L$  is defined by

$$\begin{aligned}
\Pi_L(k_0, \vec{k}) &= \Pi(k_0, \vec{k}) + \Pi(k_0, \vec{k}) \vec{k}^2 G_\pi(k_0, \vec{k}) \Pi(k_0, \vec{k}) \\
&= (k^2 - m_\pi^2) \Pi(k_0, \vec{k}) G_\pi(k_0, \vec{k}) .
\end{aligned} \tag{37}$$

## References

- [1] E.V. Shuryak, Phys. Lett. B 78 (1979) 150.
- [2] J.J. Sakurai, Ann. Phys. 11 (1960) 1.
- [3] N.M. Kroll, T.D. Lee and B. Zumino, Phys. Rev. 157 (1967) 1376.
- [4] R. Rapp and J. Wambach, preprint hep-ph/9909229, to be published in Adv. Nucl. Phys.
- [5] T. Ericson and W. Weise, Pions and Nuclei (Oxford University Press, New York, 1988).
- [6] C. Gale and J. Kapusta, Phys. Rev. C 35 (1987) 2107.
- [7] C.L. Korpa and S. Pratt, Phys. Rev. Lett. 64 (1990) 1502.
- [8] G. Chanfray and P. Schuck, Nucl. Phys. A 555 (1993) 329.
- [9] M. Herrmann, B. Friman and W. Nörenberg, Nucl. Phys. A 560 (1993) 411;  
M. Herrmann, PhD thesis, Darmstadt 1992 (GSI-Report 92-10).
- [10] B. Friman and H.J. Pirner, Nucl. Phys. A 617 (1997) 496.
- [11] W. Peters, M. Post, H. Lenske, S. Leupold and U. Mosel, Nucl. Phys. A 632 (1998) 109.
- [12] G. Agakichiev et al., CERES collaboration, Phys. Rev. Lett. 75 (1995) 1272;  
P. Wurm for the CERES collaboration, Nucl. Phys. A 590 (1995) 103c.  
G. Agakichiev et al., CERES collaboration, Phys. Lett. B 422 (1998) 405.
- [13] R. Rapp, G. Chanfray and J. Wambach, Nucl. Phys. A 617 (1997) 472.
- [14] R. Rapp and J. Wambach, preprint hep-ph/9907502.
- [15] M. Urban, M. Buballa, R. Rapp and J. Wambach, Nucl. Phys. A 641 (1998) 433.
- [16] R. Rapp, M. Urban, M. Buballa and J. Wambach, Phys. Lett. B 417 (1998) 1.
- [17] A.L. Fetter and J.D. Walecka, Quantum Theory of many-particle systems (McGraw-Hill, New York, 1971).
- [18] C. Gale and J.I. Kapusta, Nucl. Phys. B 357 (1991) 65.
- [19] R. Rapp and C. Gale, Phys. Rev. C 60 (1999) 24903.
- [20] A.B. Migdal, Rev. Mod. Phys. 50 (1978) 107.
- [21] J.F. Mathiot, Nucl. Phys. A 412 (1984) 201.
- [22] J.V. Steele, H. Yamagishi and I. Zahed, Phys. Rev. D 56 (1997) 5605.
- [23] M. Dey, V.L. Eletsky and B.L. Ioffe, Phys. Lett. B 252 (1990) 620,  
V.L. Eletsky and B.L. Ioffe, Phys. Rev. D 51 (1995) 2371.